

Linear Precoding with Low-Resolution DACs for Massive MU-MIMO-OFDM Downlink

Sven Jacobsson *Student Member, IEEE*, Giuseppe Durisi *Senior Member, IEEE*,
Mikael Coldrey *Member, IEEE*, and Christoph Studer *Senior Member, IEEE*

Abstract—We consider the downlink of a massive multiuser (MU) multiple-input multiple-output (MIMO) system in which the base station (BS) is equipped with low-resolution digital-to-analog converters (DACs). As opposed to recent results for such BS architectures, we assume that the system operates over a frequency-selective wideband channel and uses orthogonal frequency division multiplexing (OFDM) to simplify equalization at the user equipments (UEs). Furthermore, we consider the practically relevant case of oversampling DACs. We analyze the uncoded bit error rate (BER) performance with linear precoders (e.g., zero forcing) and quadrature phase-shift keying using Bussgang’s theorem. We further develop a lower bound on the information-theoretic sum-rate throughput achievable with Gaussian inputs, which can be evaluated exactly for the case of 1-bit DACs. For the case of multi-bit DACs, we derive approximate yet accurate expressions for the distortion caused by the low-resolution DACs, which can be used to evaluate the aforementioned sum-rate throughput lower bound. Our results suggest that, for a massive MU-MIMO-OFDM system with a 128-antenna BS serving 16 UEs simultaneously, only 3–4 DAC bits are required to achieve an uncoded BER of 10^{-4} with a negligible performance penalty compared to the infinite-resolution case at the cost of additional out-of-band emissions.

I. INTRODUCTION

Massive multiuser (MU) multiple-input multiple-output (MIMO), i.e., equipping the base station (BS) with hundreds of active antenna elements to serve simultaneously tens of user equipments (UEs), is widely considered a key technology in future cellular communication systems [2]. Massive MU-MIMO promises large gains in spectral efficiency and energy efficiency over traditional, small-scale MIMO systems [3]–[6], which can be achieved by simple signal processing techniques (e.g., linear precoding) at the BS [3], [4].

Increasing the number of active antenna elements at the BS by orders of magnitude inevitably leads to significant increases in circuit power consumption. Data converters,

i.e., analog-to-digital converters (ADCs) and digital-to-analog converters (DACs), are foreseen to be among the most dominant sources of power consumption in massive MU-MIMO systems. In today’s state-of-the-art MIMO systems, a pair of high-resolution DACs (e.g., with 10 bit precision) is used to generate the transmitted baseband signal at each antenna element at the BS. Scaling such architectures to massive MU-MIMO systems in which the number of antennas at the BS could be in the order of hundreds would lead to excessively high power consumption. Hence, to maintain a reasonable power budget, the resolution of the DACs must be kept low. Furthermore, equipping the BS with hundreds of active antenna elements at the BS puts extreme capacity requirements on the *fronthaul* link that connects the baseband processing unit to the radio unit (where the DACs are located). By lowering the resolution of the DACs, one can—to some extent—mitigate this fronthaul capacity bottleneck by reducing the number of bits per data sample that must be transferred to the DACs. Motivated by these results, we will consider a massive MU-MIMO *downlink* (BS transmits data to multiple UEs) system for the case in which low-resolution DACs are employed at the BS.

A. Contributions

We analyze the performance achievable on the massive MU-MIMO downlink with linear precoding and low-resolution DACs. In contrast to previous results [7]–[13], which consider symbol-rate DACs and single-carrier modulation over frequency-flat channels, we focus on oversampling DACs and orthogonal frequency division multiplexing (OFDM) modulation over frequency-selective channels. We analyze the performance of conventional linear precoders, namely maximal-ratio transmission (MRT), zero-forcing (ZF), and Wiener-filter (WF) precoding, when they are followed by low-resolution DACs. These methods are of interest because they entail low signal-processing complexity. Our contributions can be summarized as follows:

- We develop a lower bound on the information-theoretic sum-rate achievable with linear precoding and oversampling low-resolution DACs using Bussgang’s theorem [14], [15]. This lower bound can be achieved by Gaussian signaling and symbol-wise nearest-neighbor decoding at the UEs. We also show how to evaluate the lower bound for the case of 1-bit DACs using Van Vleck’s arcsine law [16].
- For the case of multi-bit DACs, we develop approximate models for the distortion caused by low-resolution DACs. The proposed models yields an accurate approximation for the signal-to-interference-noise-and-distortion

S. Jacobsson is with Ericsson Research, 41756 Gothenburg, Sweden and also with the Department of Electrical Engineering, Chalmers University of Technology, 41296 Gothenburg, Sweden (e-mail: sven.jacobsson@ericsson.com).

G. Durisi is with the Department of Electrical Engineering, Chalmers University of Technology, 41296 Gothenburg, Sweden (e-mail: durisi@chalmers.se).

M. Coldrey is with Ericsson Research, 41756 Gothenburg, Sweden (e-mail: mikael.coldrey@ericsson.com)

C. Studer is with the School of Electrical and Computer Engineering, Cornell University, Ithaca, NY 14853, USA (e-mail: studer@cornell.edu; web: http://vip.ece.cornell.edu).

The simulator used to obtain the numerical results in Section V will be made available upon (possible) acceptance of the paper.

This paper will be presented, in part, at the IEEE Global Commun. Conf. (GLOBECOM), Singapore, December 2017 [1].

ratio (SINDR) at the UEs, which we use to evaluate the aforementioned sum-rate lower bound, as well as the uncoded bit error rate (BER) that is achieved by quadrature phase-shift keying (QPSK). We also use these models to investigate the out-of-band (OOB) emissions caused by the use of low-resolution DACs.

- We demonstrate, through extensive numerical simulations, that massive MU-MIMO-OFDM with low-resolution DACs enables excellent performance in terms of achievable rate and uncoded/coded BER. Specifically, we show that few DAC bits (e.g., 3–4 bits) are sufficient to achieve the performance obtainable with infinite-resolution DACs.

B. Relevant Prior Art

1) *Residual Transmitter Impairments*: The impact of residual radio frequency (RF) hardware impairments in the massive MU-MIMO downlink has been investigated in, e.g., [17]–[20] using a model that treats the aggregate hardware impairments as power-dependent independent additive Gaussian noise. However, such crude models are not sufficiently accurate to describe the distortion caused by low-resolution DACs.

2) *Low-Resolution ADCs*: The impact of low-resolution ADCs on performance of the massive MU-MIMO *uplink* for narrowband and wideband systems has been analyzed in, e.g., [21]–[24]. These studies suggest that low-resolution ADCs can be deployed at the BS with negligible performance degradation compared to the infinite-resolution case.

3) *Low-Resolution DACs*: Recent works [7]–[9] have considered linear precoding strategies, such as MRT, ZF, and WF precoding for narrowband systems with 1-bit DACs at the BS. These works show that 1-bit-DAC massive MU-MIMO systems support low BERs and high sum-rate throughput despite the severe nonlinearity caused by the 1-bit DACs. Again for the case of 1-bit DACs, more sophisticated *nonlinear* precoding strategies that significantly outperform linear precoders at the cost of an increased signal-processing complexity were presented in [9]–[13]. It is, however, an open question whether such nonlinear precoders can be extended to the frequency-selective case with a tolerable implementation complexity.

Multi-bit DACs for the massive MU-MIMO case were considered in [9]. There, it is shown that DACs with few bits (e.g., 3–4 bits) are sufficient to close the gap to the infinite-resolution case if the BS has access to perfect channel state information (CSI). The authors of [25] developed a linear precoder, called WF-quantized (WFQ) precoding, by using an approximate model for the distortion caused by the DACs. The proposed precoder is shown to outperform conventional precoders for small-to-moderate MIMO systems at high signal-to-noise ratio (SNR). However, as shown in [9], the performance gain of the WFQ precoder over conventional linear precoders (e.g., ZF) is marginal in the massive MU-MIMO case.

All works about DACs reviewed so far dealt with the frequency-flat case. The first work to consider 1-bit DACs combined with OFDM for massive MU-MIMO is [26]. There, using an approximate model for the distortion caused by 1-bit DACs, it is shown that MRT precoding enables the use

of 1-bit DACs in massive MU-MIMO-OFDM. Recently, we used an exact model for the 1-bit-DAC distortion in [1] in order to characterize the BER achievable in an OFDM system with QPSK, as well as the sum-rate throughput achievable with a Gaussian codebook and nearest-neighbor decoding, for the case of linear precoding followed by 1-bit DACs. This paper complements the analysis in [1] by generalizing it to multi-bit DACs.

C. Notation

Lowercase and uppercase boldface letters designate column vectors and matrices, respectively. For a matrix \mathbf{A} , we denote its complex conjugate, transpose, and Hermitian transpose by \mathbf{A}^* , \mathbf{A}^T , and \mathbf{A}^H , respectively. The entry on the k th row and on the ℓ th column of the matrix \mathbf{A} is denoted as $[\mathbf{A}]_{k,\ell}$. The k th entry of a vector \mathbf{a} is denoted as $[\mathbf{a}]_k$. The trace and the main diagonal of \mathbf{A} are $\text{tr}(\mathbf{A})$ and $\text{diag}(\mathbf{A})$, respectively. The matrix $\text{diag}(\mathbf{a})$ is diagonal with the elements of the vector \mathbf{a} along its main diagonal. If \mathbf{A} is an $M \times N$ matrix, then $\text{vec}(\mathbf{A})$ is the MN -dimensional vector obtained by stacking the columns of \mathbf{A} on top of each other. The $M \times M$ identity matrix, the $M \times N$ all-zeros matrix, and the $M \times N$ all-ones matrix are denoted by \mathbf{I}_M , $\mathbf{0}_{M \times N}$, and $\mathbf{1}_{M \times N}$, respectively. The real and the imaginary parts of a complex vector \mathbf{a} are $\Re\{\mathbf{a}\}$ and $\Im\{\mathbf{a}\}$, respectively. We use $\|\mathbf{a}\|$ to denote the ℓ_2 -norm of \mathbf{a} . The Kronecker product of two matrices \mathbf{A} and \mathbf{B} is $\mathbf{A} \otimes \mathbf{B}$. We use $\text{sgn}(\cdot)$ to denote the signum function, which is applied entry-wise to vectors and defined as $\text{sgn}(a) = 1$ if $a \geq 0$ and $\text{sgn}(a) = -1$ if $a < 0$. We further use $\mathbb{1}_{\mathcal{A}}(a)$ to denote the indicator function, which is defined as $\mathbb{1}_{\mathcal{A}}(a) = 1$ for $a \in \mathcal{A}$ and $\mathbb{1}_{\mathcal{A}}(a) = 0$ for $a \notin \mathcal{A}$. The multivariate complex-valued circularly-symmetric Gaussian distribution with covariance matrix \mathbf{K} is denoted by $\mathcal{CN}(\mathbf{0}, \mathbf{K})$. We use $\mathbb{P}[\mathcal{E}]$ to denote the probability of the event \mathcal{E} and $\mathbb{E}_x[\cdot]$ to denote expectation with respect to the random variable x . Finally, the function $\Phi(x) = \frac{1}{\sqrt{2\pi}} \int_{-\infty}^x \exp(-u^2/2) du$ is the cumulative distribution function of the standard normal distribution.

D. Paper Outline

The rest of the paper is organized as follows. In Section II, we introduce the system model as well as the considered precoding schemes, and we describe the operation of the DACs. In Section III, we review Busgang's theorem, derive the SINDR at the UEs, and develop a lower bound on the rate achievable with Gaussian inputs and nearest-neighbor decoding. In Section IV, we derive exact and approximate expressions for the distortion caused by finite-resolution DACs; we then use these expressions to evaluate the achievable-rate lower bound from Section III and the uncoded BER achievable with QPSK. In Section V, we provide numerical simulations that demonstrate the accuracy of our analytical results. We conclude the paper in Section VI. All proofs are relegated to the appendices.

II. SYSTEM MODEL

We consider the single-cell downlink massive MU-MIMO-OFDM system depicted in Fig. 1. The system consists of

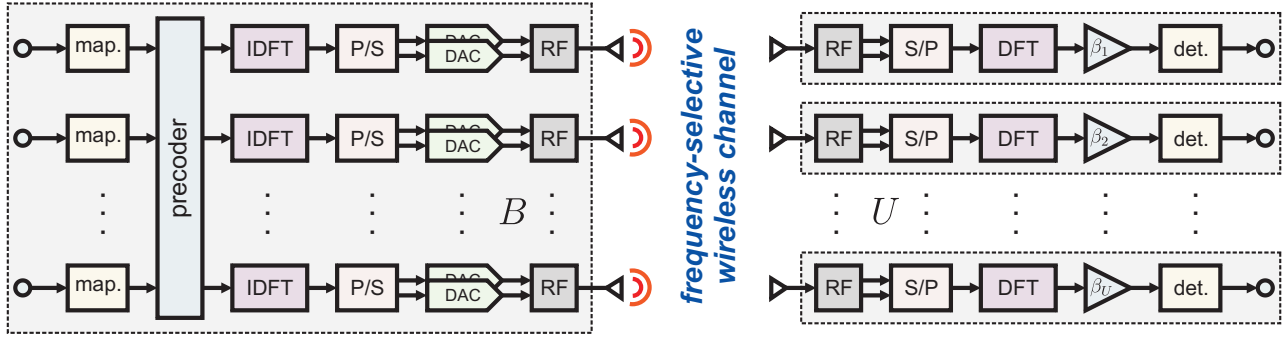


Fig. 1. Overview of the studied massive MU-MIMO-OFDM downlink with low-resolution DACs at the BS. Left: A B antenna BS performs linear precoding and generates the per-antenna OFDM time-domain signals that are passed through low-resolution DACs. Right: U single-antenna UEs perform independently OFDM demodulation and data detection. In the figure, “map.” and “det.” stand for mapper and detector, respectively.

a BS with B antennas that simultaneously serves U single-antenna UEs in the same time-frequency resource through spatial multiplexing. Our model includes low-resolution DACs at the BS. Specifically, the in-phase and quadrature components of the time-domain per-antenna transmitted signal at the BS are generated using a pair of low-resolution DACs. Let $\mathcal{L} = \{\ell_0, \dots, \ell_{L-1}\}$, where $\ell_0 < \ell_1 < \dots < \ell_{L-2} < \ell_{L-1}$, denote the set of possible DAC outcomes, i.e., the set of possible amplitude (voltage) levels that are supported by the transcoder in the DACs. The DACs have finite resolution, and hence, the set \mathcal{L} has finite cardinality. We refer to $L = |\mathcal{L}|$ and to $\log_2(L)$ as the number of DAC *levels* and as the number of DAC *bits* per real dimension, respectively. We assume all DACs in the system to be the same. Hence, the set of complex-valued DAC outputs at each antenna is $\mathcal{X} = \mathcal{L} \times \mathcal{L}$.

We assume that the system operates over a wideband channel and that OFDM is used to mitigate the frequency selectiveness of the channel. Specifically, at the BS, the frequency-domain precoded vector is mapped to time domain by performing an inverse discrete Fourier transform (IDFT) at each antenna element. At the UEs, the time-domain received signal is mapped back to frequency domain through a discrete Fourier transform (DFT). Unfortunately, the nonlinearity introduced by the finite-resolution DACs yields intercarrier interference (ICI).

A. OFDM Numerology

We assume that each OFDM symbol consists of S data symbols and N time samples. Let Δf be the subcarrier spacing and $f_s = N\Delta f$ be the sampling rate of the DACs. We use the disjoint sets \mathcal{S}_d and \mathcal{S}_g to denote the set of subcarriers designated for data symbols (occupied subcarriers) and the set of guard subcarriers, respectively. The number of occupied subcarriers is $|\mathcal{S}_d| = S$, and the number of guard subcarriers is $|\mathcal{S}_g| = N - S$. Let \mathbf{s}_k denote the U -dimensional data vector associated with the k th ($k = 0, \dots, N-1$) subcarrier. We shall assume that $\mathbf{s}_k = \mathbf{0}_{U \times 1}$ for $k \in \mathcal{S}_g$ and that $\mathbb{E}[\mathbf{s}_k \mathbf{s}_k^H] = \mathbf{I}_U$ for $k \in \mathcal{S}_d$. Note that the case $S = N$ corresponds to symbol-rate DACs whereas setting $S < N$ corresponds to oversampling DACs. We define the oversampling ratio (OSR) as $\xi = N/S$.

B. Channel Input-Output Relation

For simplicity, we shall assume that all RF circuitry other than the DACs (e.g., local oscillators, mixers, power amplifiers, etc.) are ideal and that the UEs are equipped with ADCs of infinite resolution. We further assume that the sampling rate f_s of the DACs at the BS equals the sampling rate of the ADCs at the UEs and that the system is perfectly synchronized. Finally, we assume that the *reconstruction stage* (see, e.g., [27]) of the DACs is an ideal low-pass filter with cut-off frequency $f_s/2$.¹

1) *Time Domain*: If the above assumptions are satisfied, then the discrete-time baseband signal $\mathbf{y}_n \in \mathbb{C}^U$ received at the U UEs at time sample n can be written as

$$\mathbf{y}_n = \sum_{t=0}^{T-1} \mathbf{H}_t \mathbf{x}_{n-t} + \mathbf{w}_n \quad (1)$$

for $n = 0, \dots, N-1$. Here, $\mathbf{x}_n \in \mathcal{X}^B$ is the transmitted signal (i.e., the output of the DACs) at time sample n . The random vector $\mathbf{w}_n \sim \mathcal{CN}(\mathbf{0}_{U \times 1}, N_0 \mathbf{I}_U)$ models the additive white Gaussian noise (AWGN) at the u th UE at time sample n . Here, N_0 is the power spectral density (PSD) of the AWGN. The matrix $\mathbf{H}_t \in \mathbb{C}^{U \times B}$ is the time-domain channel matrix associated with the t th tap of the frequency-selective channel ($t = 0, \dots, T-1$, where T is the number of taps). We assume that this matrix has entries $[\mathbf{H}_t]_{u,b} \sim \mathcal{CN}(0, 1/\sqrt{T})$, and that the entries of $\{\mathbf{H}_t\}$ are independent and remain constant for the duration of an OFDM symbol. Note that these assumptions yield a spatially white frequency-selective Rayleigh-fading channel with uniform power-delay profile.

The transmitted signal $\{\mathbf{x}_n\}$ must satisfy the following average power constraint:

$$\mathbb{E} \left[\sum_{n=0}^{N-1} \|\mathbf{x}_n\|^2 \right] \leq PS. \quad (2)$$

Here, $0 < P < \infty$ is the average transmit power at the BS. We define $\rho = P/N_0$ as the signal-to-noise ratio (SNR).

A cyclic prefix of length $T-1$ is prepended to the transmitted signal and is later discarded at the UEs. We shall not explicitly prepend the cyclic prefix to $\{\mathbf{x}_n\}$ to keep notation compact.

¹As we shall see later, low-resolution DACs cause undesired OOB emissions that may be mitigated via analog filters. Such filters may, however, cause ICI.

The cyclic prefix makes the channel matrix circulant and, hence, diagonalizable through an IDFT and a DFT at the BS and at the UEs, respectively.

2) *Frequency Domain*: Let $\mathbf{X} = [\mathbf{x}_0, \dots, \mathbf{x}_{N-1}] \in \mathcal{X}^{B \times N}$ and $\mathbf{Y} = [\mathbf{y}_0, \dots, \mathbf{y}_{N-1}] \in \mathbb{C}^{U \times N}$ be the time-domain transmitted and received matrices over the N time samples, respectively. Furthermore, let $\widehat{\mathbf{X}} = \mathbf{X}\mathbf{F}^T$ and $\widehat{\mathbf{Y}} = \mathbf{Y}\mathbf{F}^T$ be the corresponding frequency-domain matrices. Here, \mathbf{F} stands for the $N \times N$ DFT matrix, which satisfies $\mathbf{F}\mathbf{F}^H = \mathbf{I}_N$. Finally, let

$$\widehat{\mathbf{H}}_k = \sum_{t=0}^{T-1} \mathbf{H}_t \exp\left(-jk \frac{2\pi}{N} t\right) \quad (3)$$

for $k = 0, \dots, N-1$, be the $U \times B$ frequency-domain channel matrix associated with the k th subcarrier.

After discarding the cyclic prefix, we can write the frequency-domain input-output relation at the k th subcarrier as

$$\widehat{\mathbf{y}}_k = \widehat{\mathbf{H}}_k \widehat{\mathbf{x}}_k + \widehat{\mathbf{w}}_k. \quad (4)$$

Here, $\widehat{\mathbf{x}}_k$ and $\widehat{\mathbf{y}}_k$ are the k th column of $\widehat{\mathbf{X}}$ and $\widehat{\mathbf{Y}}$, respectively. Furthermore, $\widehat{\mathbf{w}}_k \sim \mathcal{CN}(\mathbf{0}_{U \times 1}, N_0 \mathbf{I}_U)$ is the k th column of the matrix $\widehat{\mathbf{W}} = \mathbf{W}\mathbf{F}^T$, where $\mathbf{W} = [\mathbf{w}_0, \dots, \mathbf{w}_{N-1}]$.

In the following two subsections, we shall relate the frequency-domain representation $\widehat{\mathbf{x}}_k$ of the DAC output to the precoded transmitted symbols.

C. Uniform Quantization

For the discrete-time system model (1) considered in this paper, each DAC can be modeled simply as a *quantizer*, i.e., a nonlinear device that maps a continuous-amplitude signal to a set of discrete numbers [28].² We characterize the quantizer by the set $\mathcal{L} = \{\ell_0, \dots, \ell_{L-1}\}$ of L quantization labels and the set $\mathcal{T} = \{\tau_0, \dots, \tau_L\}$, where $-\infty = \tau_0 < \tau_1 < \dots < \tau_{L-1} < \tau_L = \infty$, of $L+1$ quantization thresholds. We use the *quantization function* $\mathcal{Q}(\cdot) : \mathbb{C}^B \rightarrow \mathcal{X}^B$ to describe the joint operation of the $2B$ DACs at the BS.³ Let $\mathbf{z}_n \in \mathbb{C}^B$ denote the time-domain precoded vector at time sample n .⁴ Also, let $z_{b,n} = [\mathbf{z}_n]_b$ and $x_{b,n} = [\mathbf{x}_n]_b$. Then,

$$\mathcal{Q}(z_{b,n}) = \sum_{i=0}^{L-1} \ell_i \mathbb{1}_{[\tau_i, \tau_{i+1})}(z_{b,n}^R) + j \sum_{i=0}^{L-1} \ell_i \mathbb{1}_{[\tau_i, \tau_{i+1})}(z_{b,n}^I) \quad (5)$$

where $z_{b,n}^R = \Re\{z_{b,n}\}$ and $z_{b,n}^I = \Im\{z_{b,n}\}$. For simplicity, we shall model the DACs as symmetric *uniform* quantizers (the labels $\{\ell_i\}$ are equispaced and symmetric around zero) with step size Δ . For symmetric uniform quantizers, the quantization thresholds are given by

$$\tau_i = \Delta \left(i - \frac{L}{2} \right) \quad (6)$$

²This model assumes that the reconstruction stage [27] of each DAC is an ideal low-pass filter.

³We assume that the baseband processing unit at the BS uses floating-point arithmetic with infinite word length. The impact of having finite word lengths in massive MU-MIMO baseband processing has been investigated in [29].

⁴In Section II-D, we shall describe how this vector is obtained from the data symbols $\{\mathbf{s}_k\}$ for $k \in \mathcal{S}_d$.

for $i = 1, \dots, L-1$, with $\tau_0 = -\infty$ and $\tau_L = \infty$. Furthermore, the quantization labels are given by

$$\ell_i = \alpha \Delta \left(i - \frac{L-1}{2} \right) \quad (7)$$

for $i = 0, \dots, L-1$. The quantization labels in (7) are scaled by a constant α to ensure that the transmit power constraint (2) is satisfied.

If L is odd, the quantizer has a label at zero; we shall refer to such quantizers as a *midtreed* quantizer. If L is even, the quantizer has a threshold at zero; we shall refer to such quantizers as a *midrise* quantizer.

The choice of the step size Δ impacts the amount of distortion caused by the DACs. If Δ is too small, there will be significant *overload* distortion (clipping or saturation), whereas if Δ is too large there will be significant *granular* distortion. Specifically, let $A_{\text{clip}} = L\Delta/2$ be the *clipping level* of the uniform quantizer. Overload distortion is the quantization error $\alpha^{-1}\mathcal{Q}(z) - z$ occurring if $|z| > A_{\text{clip}}$. Granular distortion, on the other hand, is the quantization error $\alpha^{-1}\mathcal{Q}(z) - z$ occurring if $|z| \leq A_{\text{clip}}$. As we shall see, it will be important for our analysis to keep the overload distortion small. Therefore, we shall choose the step size Δ such that the probability of the event $|z| > A_{\text{clip}}$ is small. We shall return to this point in Sections IV-C and V.

In the extreme case of 1-bit DACs, the quantization function (5) reduces to

$$\mathcal{Q}(z_{b,n}) = \frac{\alpha \Delta}{2} (\text{sgn}(z_{b,n}^R) + j \text{sgn}(z_{b,n}^I)). \quad (8)$$

In this case, by setting

$$\alpha = \sqrt{\frac{2P}{\Delta^2 \xi B}} \quad (9)$$

we ensure that the power constraint (2) is satisfied with equality.

D. Linear Precoding

At the BS, the data symbols for the U UEs are mapped to the antenna array by a precoder. For analytical tractability and to limit computational complexity, we shall focus, in this paper, only on linear precoders. Linear precoders—although inferior in performance to nonlinear precoders [4]—are attractive in massive MU-MIMO-OFDM systems due to the simple signal processing that these methods entail. Furthermore, it has been demonstrated that linear precoders offer near-optimal performance for large antenna arrays [4].

We assume that the BS has access to perfect CSI, i.e., it has perfect knowledge of the realizations of the frequency-domain channel matrices $\{\widehat{\mathbf{H}}_k\}$ for $k \in \mathcal{S}_d$. With linear precoding, the transmitted vector \mathbf{x}_n can be written as

$$\mathbf{x}_n = \mathcal{Q}(\mathbf{z}_n) \quad (10)$$

where $\mathbf{z}_n \in \mathbb{C}^B$ denotes the time-domain precoded vector at time sample n , which is obtained from the data symbols $\{\mathbf{s}_k\}_{k \in \mathcal{S}_d}$ as follows:

$$\mathbf{z}_n = \frac{1}{\sqrt{N}} \sum_{k \in \mathcal{S}_d} \widehat{\mathbf{P}}_k \mathbf{s}_k \exp\left(jk \frac{2\pi}{N} n\right). \quad (11)$$

for $n = 0, \dots, N - 1$. In words, the data symbols on the k th subcarrier ($k \in \mathcal{S}_d$) are multiplied in the frequency domain with the *precoding matrix* $\hat{\mathbf{P}}_k \in \mathbb{C}^{B \times U}$. The resulting frequency-domain precoded vector is then mapped to time domain by an IDFT. We use the convention that $\hat{\mathbf{P}}_k = \mathbf{0}_{B \times U}$ for $k \in \mathcal{S}_g$.

In this work, we shall consider three different linear precoders that are commonly used in the infinite-resolution case. More specifically, we shall analyze the performance of MRT, ZF, and WF precoding.

1) *WF precoding*: By assuming infinite-resolution DACs at the BS and by minimizing the mean square error (MSE) between the transmitted and received symbols, one obtains the WF precoder [30]

$$\hat{\mathbf{P}}_k^{\text{WF}} = \frac{1}{\beta^{\text{WF}}} \hat{\mathbf{H}}_k^H \left(\hat{\mathbf{H}}_k \hat{\mathbf{H}}_k^H + \frac{UN_0}{P} \mathbf{I}_U \right)^{-1} \quad (12)$$

where $k \in \mathcal{S}_d$. Here, β^{WF} is a constant that ensures that the power constraint (2) is satisfied (in the infinite-resolution case):

$$\beta^{\text{WF}} = \left(\frac{1}{PS} \sum_{k \in \mathcal{S}_d} \text{tr} \left(\left(\hat{\mathbf{H}}_k \hat{\mathbf{H}}_k^H + \frac{UN_0}{P} \mathbf{I}_U \right)^{-1} \times \hat{\mathbf{H}}_k \hat{\mathbf{H}}_k^H \left(\hat{\mathbf{H}}_k \hat{\mathbf{H}}_k^H + \frac{UN_0}{P} \mathbf{I}_U \right)^{-1} \right) \right)^{1/2}. \quad (13)$$

2) *ZF precoding*: With ZF precoding, the BS nulls the MU interference by choosing as precoding matrix the pseudo-inverse of the channel matrix. The ZF precoding matrix is obtained from (12) by setting the noise PSD N_0 to zero, which yields

$$\hat{\mathbf{P}}_k^{\text{ZF}} = \frac{1}{\beta^{\text{ZF}}} \hat{\mathbf{H}}_k^H \left(\hat{\mathbf{H}}_k \hat{\mathbf{H}}_k^H \right)^{-1} \quad (14)$$

for $k \in \mathcal{S}_d$, where

$$\beta^{\text{ZF}} = \sqrt{\frac{1}{PS} \sum_{k \in \mathcal{S}_d} \text{tr} \left(\hat{\mathbf{H}}_k \hat{\mathbf{H}}_k^H \right)^{-1}} \quad (15)$$

ensures that the power constraint (2) is satisfied (in the infinite-resolution case).

3) *MRT precoding*: The MRT precoder maximizes the power directed towards each UE, ignoring MU interference. The MRT precoding matrix can be obtained from (12) by letting the noise variance N_0 tend to infinity, which yields

$$\hat{\mathbf{P}}_k^{\text{MRT}} = \frac{1}{\beta^{\text{MRT}} B} \hat{\mathbf{H}}_k^H \quad (16)$$

for $k \in \mathcal{S}_d$, where

$$\beta^{\text{MRT}} = \frac{1}{B} \sqrt{\frac{1}{PS} \sum_{k \in \mathcal{S}_d} \text{tr} \left(\hat{\mathbf{H}}_k \hat{\mathbf{H}}_k^H \right)} \quad (17)$$

ensures that the power constraint (2) is satisfied (in the infinite-resolution case)

III. PERFORMANCE ANALYSIS

In the infinite-resolution case, the frequency-domain received signal $\hat{\mathbf{y}}_k$ in (4) under linear precoding can be written as

$$\hat{\mathbf{y}}_k = \hat{\mathbf{H}}_k \hat{\mathbf{P}}_k \mathbf{s}_k + \hat{\mathbf{w}}_k. \quad (18)$$

In words, the received signal on subcarrier $k \in \mathcal{S}_d$ depends only on \mathbf{s}_k and not on the data symbols transmitted on other subcarriers. Hence, each subcarrier can be analyzed separately. In the finite-resolution-DAC case, however, the nonlinearity introduced by the finite-resolution DACs through (5) makes the received signal on one subcarrier depend, in general, on the data symbols transmitted on all other subcarriers. For performance analyses, it is convenient to write the frequency-domain received signal $\hat{\mathbf{Y}}$ in vectorized form $\hat{\mathbf{y}} = \text{vec}(\hat{\mathbf{Y}}) \in \mathbb{C}^{UN}$ as

$$\hat{\mathbf{y}} = \hat{\mathbf{H}} \hat{\mathbf{x}} + \hat{\mathbf{w}}. \quad (19)$$

Here, $\hat{\mathbf{x}} = \text{vec}(\hat{\mathbf{X}}) \in \mathbb{C}^{BN}$, $\hat{\mathbf{w}} = \text{vec}(\hat{\mathbf{W}}) \in \mathbb{C}^{UN}$, and $\hat{\mathbf{H}}$ is the $UN \times BN$ block-diagonal matrix that has the matrices $\hat{\mathbf{H}}_0, \dots, \hat{\mathbf{H}}_{N-1}$ on its main diagonal. We next observe that we can rewrite $\hat{\mathbf{x}}$ as

$$\hat{\mathbf{x}} = \text{vec}(\hat{\mathbf{X}}) = \text{vec}(\mathbf{X}\mathbf{F}^T) = (\mathbf{F} \otimes \mathbf{I}_B) \mathbf{x} \quad (20)$$

where $\mathbf{x} = \text{vec}(\mathbf{X})$. In (20), the quantized time-domain precoded vector \mathbf{x} is given by $\mathbf{x} = \mathcal{Q}(\mathbf{z})$ where $\mathbf{z} = \text{vec}(\mathbf{Z}) \in \mathbb{C}^{BN}$ and where $\mathbf{Z} = [\mathbf{z}_0, \dots, \mathbf{z}_{N-1}]$. Now let $\hat{\mathbf{P}} \in \mathbb{C}^{BN \times UN}$ denote the block-diagonal matrix that has the matrices $\hat{\mathbf{P}}_0, \dots, \hat{\mathbf{P}}_{N-1}$ on its main diagonal. With these definitions, we can write the infinite-resolution time-domain precoded vector \mathbf{z} as

$$\mathbf{z} = (\mathbf{F}^H \otimes \mathbf{I}_B) \hat{\mathbf{P}} \mathbf{s} \quad (21)$$

where $\mathbf{s} = \text{vec}(\mathbf{S})$, and where $\mathbf{S} = [\mathbf{s}_0, \dots, \mathbf{s}_{N-1}]$. Now, using (20) and (21) in (19), we obtain

$$\hat{\mathbf{y}} = \hat{\mathbf{H}} (\mathbf{F} \otimes \mathbf{I}_B) \mathcal{Q} \left((\mathbf{F}^H \otimes \mathbf{I}_B) \hat{\mathbf{P}} \mathbf{s} \right) + \hat{\mathbf{w}}. \quad (22)$$

Comparing (18) and (22), we see how the nonlinearity introduced by $\mathcal{Q}(\cdot)$ complicates the input-output relation by introducing ICI, thus, preventing a straightforward evaluation of the performance of the MU-MIMO-OFDM downlink system. In the next section, we shall use Bussgang's theorem [14] to decompose (22) into a form that enables an analytical analysis.

A. Decomposition Using Bussgang's Theorem

The finite-resolution DACs introduce a quantization error $\mathbf{e} \in \mathbb{C}^{BN}$, which is given by

$$\mathbf{e} = \alpha^{-1} \mathbf{x} - \mathbf{z} = \alpha^{-1} \mathcal{Q}(\mathbf{z}) - \mathbf{z}. \quad (23)$$

The division by α is required because we scaled the quantization labels in (7) by α to satisfy the power constraint (2). Note that \mathbf{e} is *correlated* with the quantizer input \mathbf{z} . In fact, \mathbf{e} is a deterministic function of \mathbf{z} . For Gaussian inputs, Bussgang's theorem [14] allows us to decompose $\mathcal{Q}(\mathbf{z})$ into two components: a linear function of \mathbf{z} and a distortion that is *uncorrelated* with \mathbf{z} . Specifically, assume that $\mathbf{s}_k \sim \mathcal{CN}(\mathbf{0}_{U \times 1}, \mathbf{I}_U)$ for all $k \in \mathcal{S}_d$, and that the $\{\mathbf{s}_k\}_{k \in \mathcal{S}_d}$ are independent. By using Bussgang's theorem, the transmitted time-domain vector \mathbf{x} can be written as [9], [15]

$$\mathbf{x} = \mathcal{Q}(\mathbf{z}) = \mathbf{G} \mathbf{z} + \mathbf{d} \quad (24)$$

where the distortion $\mathbf{d} \in \mathbb{C}^{BN}$ is uncorrelated with \mathbf{z} , i.e., $\mathbb{E}[\mathbf{z} \mathbf{d}^H] = \mathbf{0}_{B \times B}$. Furthermore, $\mathbf{G} \in \mathbb{R}^{BN \times BN}$ is the

diagonal matrix given by

$$\mathbf{G} = \mathbf{I}_N \otimes \text{diag}(\mathbf{g}) \quad (25)$$

where $\text{diag}(\mathbf{g}) \in \mathbb{R}^{B \times B}$ is (cf. [9, Eq. (14)])

$$\begin{aligned} \text{diag}(\mathbf{g}) &= \frac{\alpha \Delta}{\sqrt{\pi}} \text{diag} \left(\frac{1}{N} \sum_{k \in \mathcal{S}_d} \hat{\mathbf{P}}_k \hat{\mathbf{P}}_k^H \right)^{-1/2} \\ &\times \sum_{i=1}^{L-1} \exp \left(-\Delta^2 \left(i - \frac{L}{2} \right)^2 \right) \\ &\times \text{diag} \left(\frac{1}{N} \sum_{k \in \mathcal{S}_d} \hat{\mathbf{P}}_k \hat{\mathbf{P}}_k^H \right)^{-1}. \end{aligned} \quad (26)$$

For the special case of 1-bit DACs, (26) reduces to

$$\text{diag}(\mathbf{g}) = \sqrt{\frac{2P}{\pi \xi B}} \text{diag} \left(\frac{1}{N} \sum_{k \in \mathcal{S}_d} \hat{\mathbf{P}}_k \hat{\mathbf{P}}_k^H \right)^{-1/2}. \quad (27)$$

Inserting (24) into (22), we obtain

$$\hat{\mathbf{y}} = \hat{\mathbf{H}}(\mathbf{F} \otimes \mathbf{I}_B) \left(\mathbf{G}(\mathbf{F}^H \otimes \mathbf{I}_B) \hat{\mathbf{P}}\mathbf{s} + \mathbf{d} \right) + \hat{\mathbf{w}} \quad (28)$$

$$= \hat{\mathbf{H}}\mathbf{G}\hat{\mathbf{P}}\mathbf{s} + \hat{\mathbf{H}}(\mathbf{F} \otimes \mathbf{I}_B) \mathbf{d} + \hat{\mathbf{w}} \quad (29)$$

where last step follows because $(\mathbf{F} \otimes \mathbf{I}_B) \mathbf{G}(\mathbf{F}^H \otimes \mathbf{I}_B) = \mathbf{G}$, since \mathbf{G} has the form given in (25).

B. Achievable Sum-Rate Throughput with Gaussian Inputs

Let $\hat{y}_{u,k} = [\hat{\mathbf{y}}_k]_u$ denote the received signal on the k th subcarrier at the u th UE. It follows from (22) that

$$\begin{aligned} \hat{y}_{u,k} &= \left[\hat{\mathbf{H}}_k \text{diag}(\mathbf{g}) \hat{\mathbf{P}}_k \right]_{u,u} s_{u,k} \\ &+ \sum_{v \neq u} \left[\hat{\mathbf{H}}_k \text{diag}(\mathbf{g}) \hat{\mathbf{P}}_k \right]_{u,v} s_{v,k} \\ &+ \left[\hat{\mathbf{H}}(\mathbf{F} \otimes \mathbf{I}_B) \mathbf{d} \right]_{u+kU} + \hat{w}_{u,k} \end{aligned} \quad (30)$$

where $s_{u,k} = [\mathbf{s}_k]_u$ and $\hat{w}_{u,k} = [\hat{\mathbf{w}}_k]_u$. The first term on the right-hand side (RHS) of (30) corresponds to the desired signal; the second term captures the MU interference; the third term describes the distortion introduced by the DACs; the fourth term represents the AWGN.

Let now $\gamma_{u,k}(\hat{\mathbf{H}})$ be the SINDR on the k th subcarrier for the u th UE. Using (30) and assuming that $\mathbf{s}_k \sim \mathcal{CN}(\mathbf{0}_{U \times 1}, \mathbf{I}_U)$ for $k \in \mathcal{S}_d$, we can express $\gamma_{u,k}(\hat{\mathbf{H}})$ as

$$\gamma_{u,k}(\hat{\mathbf{H}}) = \frac{\left[\hat{\mathbf{H}}_k \text{diag}(\mathbf{g}) \hat{\mathbf{P}}_k \right]_{u,u}^2}{\sum_{v \neq u} \left[\hat{\mathbf{H}}_k \text{diag}(\mathbf{g}) \hat{\mathbf{P}}_k \right]_{u,v}^2 + D_{u,k}(\hat{\mathbf{H}}) + N_0} \quad (31)$$

where

$$D_{u,k}(\hat{\mathbf{H}}) = \left[\hat{\mathbf{H}}(\mathbf{F} \otimes \mathbf{I}_B) \mathbf{C}_d (\mathbf{F}^H \otimes \mathbf{I}_B) \hat{\mathbf{H}}^H \right]_{u+kU, u+kU} \quad (32)$$

with $\mathbf{C}_d = \mathbb{E}[\mathbf{d}\mathbf{d}^H] \in \mathbb{C}^{BN \times BN}$ being the covariance of the distortion \mathbf{d} .

Through standard manipulations of the mutual information (see, e.g., [9]), we obtain a lower bound $\underline{R}_{\text{sum}}$ on the

sum-rate throughput that is explicit in the SINDR (31) as

$$\underline{R}_{\text{sum}} = \frac{1}{S} \mathbb{E} \left[\sum_{k \in \mathcal{S}_d} \sum_{u=1}^U \log_2 \left(1 + \gamma_{u,k}(\hat{\mathbf{H}}) \right) \right] \quad (33)$$

where the expectation is over the channel matrix $\hat{\mathbf{H}}$.

The lower bound in (33) corresponds to the rate achievable using a Gaussian codebook and a mismatched nearest-neighbor decoder at the UEs [31], [32] under the assumption that the $\{\gamma_{u,k}(\hat{\mathbf{H}})\}_{k \in \mathcal{S}_d}$ are known to UE u (for $u = 1, \dots, U$).

IV. EXACT AND APPROXIMATE DISTORTION MODELS

We next tackle the problem of evaluating the covariance matrix \mathbf{C}_d of the distortion \mathbf{d} , which is needed to compute (32) and, hence, the achievable rate (33). As in the previous section, we assume Gaussian signaling, i.e., that $\mathbf{s}_k \sim \mathcal{CN}(\mathbf{0}_{U \times 1}, \mathbf{I}_U)$ for $k \in \mathcal{S}_d$. This implies that the input \mathbf{z} of each DAC follows a $\mathcal{CN}(\mathbf{0}_{BN \times 1}, \mathbf{C}_z)$ distribution where

$$\mathbf{C}_z = (\mathbf{F}^H \otimes \mathbf{I}_B) \hat{\mathbf{P}} \hat{\mathbf{P}}^H (\mathbf{F} \otimes \mathbf{I}_B). \quad (34)$$

Since the vectors \mathbf{z} and \mathbf{d} are uncorrelated, it follows from (24) that

$$\mathbf{C}_d = \mathbf{C}_x - \mathbf{G}\mathbf{C}_z\mathbf{G}. \quad (35)$$

Here, we used that $\mathbf{G}^H = \mathbf{G}$ since \mathbf{G} is a real-valued diagonal matrix. Hence, to evaluate \mathbf{C}_d , one has to compute the covariance $\mathbf{C}_x = \mathbb{E}[\mathbf{x}\mathbf{x}^H] \in \mathbb{C}^{BN \times BN}$ of the DAC output. We shall discuss how to evaluate \mathbf{C}_x in the following sections.

A. Computation of \mathbf{C}_x

Let x_m be the m th element of \mathbf{x} . Then, we can write the entry on the m th row and n th column of \mathbf{C}_x as $\mathbb{E}[x_m x_n^*]$. Let now $x_m^R = \Re\{x_m\}$ and $x_m^I = \Im\{x_m\}$ denote the real and imaginary components of x_m , respectively. Since the input to the DACs is a circularly-symmetric Gaussian random variable, $\mathbb{E}[x_m x_n^*]$ can be as expanded as follows:

$$\mathbb{E}[x_m x_n^*] = 2 \left(\mathbb{E}[x_m^R x_n^R] + j \mathbb{E}[x_m^I x_n^R] \right). \quad (36)$$

Let now $z_m = [\mathbf{z}]_m$ and $z_m^R = \Re\{z_m\}$. For the case $m = n$, (36) reduces to

$$\mathbb{E}[|x_m|^2] = 2 \mathbb{E} \left[(x_m^R)^2 \right] \quad (37)$$

$$= 2 \sum_{i=0}^{L-1} \ell_i^2 \mathbb{P}[x_m^R = \ell_i] \quad (38)$$

$$= 2 \sum_{i=0}^{L-1} \ell_i^2 \mathbb{P}[\tau_i \leq z_m^R < \tau_{i+1}] \quad (39)$$

$$= 2 \sum_{i=0}^{L-1} \ell_i^2 \left(\Phi \left(\frac{\sqrt{2} \tau_{i+1}}{\sigma_m} \right) - \Phi \left(\frac{\sqrt{2} \tau_i}{\sigma_m} \right) \right) \quad (40)$$

$$= \frac{\alpha^2 \Delta^2}{2} (L-1)^2 - 4\alpha^2 \Delta^2 \sum_{i=1}^{L-1} \left(i - \frac{L}{2} \right) \Phi \left(\frac{\sqrt{2}}{\sigma_m} \left(i - \frac{L}{2} \right) \right) \quad (41)$$

where (40) follows because $z_m \sim \mathcal{CN}(0, \sigma_m^2)$ with $\sigma_m^2 = [\mathbf{C}_z]_{m,m}$. To derive (41), we inserted (6) and (7) into (40), and used that for uniform quantizers it holds that $\ell_{i+1} = \ell_i + \alpha\Delta$ for $i \in \{0, \dots, L-2\}$.

For the case $m \neq n$, the expectation $\mathbb{E}[x_m^C x_n^R]$, where $C \in \{R, I\}$, can be written as

$$\mathbb{E}[x_m^C x_n^R] = \sum_{a=0}^{L-1} \sum_{b=0}^{L-1} \ell_a \ell_b \mathbb{P}[x_m^C = \ell_a, x_n^R = \ell_b]. \quad (42)$$

Unfortunately, (42) does not admit in general a closed-form solution and has to be evaluated using numerical methods. One exception is the special case of 1-bit DACs, for which it can be shown that (see, e.g., [33])

$$\begin{aligned} \mathbb{P}[x_m^C = \ell_a, x_n^R = \ell_b] &= \begin{cases} \frac{1}{4} + \frac{1}{2\pi} \arcsin\left(\frac{\sigma_{m,n}^C}{\sigma_m \sigma_n}\right), & \text{if } \ell_a = \ell_b, \\ \frac{1}{4} - \frac{1}{2\pi} \arcsin\left(\frac{\sigma_{m,n}^C}{\sigma_m \sigma_n}\right), & \text{if } \ell_a \neq \ell_b. \end{cases} \end{aligned} \quad (43)$$

Here, we have defined $\sigma_{m,n}^R = \Re\{\mathbf{C}_z\}_{m,n}$ and $\sigma_{m,n}^I = \Im\{\mathbf{C}_z\}_{m,n}$. In this case, substituting (43) into (42), (42) into (36), and recalling that $\ell_1 = -\ell_0 = \sqrt{P/(2\xi B)}$, we obtain

$$\begin{aligned} \mathbb{E}[x_m x_n^*] &= \frac{2P}{\pi\xi B} \left(\arcsin\left(\frac{\sigma_{m,n}^R}{\sigma_m \sigma_n}\right) + j \arcsin\left(\frac{\sigma_{m,n}^I}{\sigma_m \sigma_n}\right) \right). \end{aligned} \quad (44)$$

This well-known result for 1-bit DACs, reported first by Van Vleck and Middleton [16], is commonly referred to as the *arcsine law*. Writing (44) in matrix form, we obtain

$$\begin{aligned} \mathbf{C}_x &= \frac{2P}{\pi\xi B} \left(\arcsin\left(\text{diag}(\mathbf{C}_z)^{-\frac{1}{2}} \Re\{\mathbf{C}_z\} \text{diag}(\mathbf{C}_z)^{-\frac{1}{2}}\right) \right. \\ &\quad \left. + j \arcsin\left(\text{diag}(\mathbf{C}_z)^{-\frac{1}{2}} \Im\{\mathbf{C}_z\} \text{diag}(\mathbf{C}_z)^{-\frac{1}{2}}\right) \right). \end{aligned} \quad (45)$$

By inserting (45) into (35) we find the desired covariance matrix \mathbf{C}_d , which allow us to compute the SINDR (31) and the rate (33).

To evaluate (35) for the general case $L > 2$, one has to solve (42) by numerical integration, which is time consuming and offers limited insights. In what follows, we shall present two closed-form approximations for \mathbf{C}_x , which trade accuracy for complexity in different ways.

B. Diagonal Approximation

The first approximation models the distortion caused by the DACs as a white process, both in the spectral and in the spatial domain, by assuming that the off-diagonal elements of \mathbf{C}_d are zero. In this case, we get that

$$\mathbf{C}_d \approx \text{diag}(\mathbf{C}_d) \quad (46)$$

$$\begin{aligned} &= \text{diag}(\mathbf{C}_x) - \mathbf{G} \text{diag}(\mathbf{C}_z) \mathbf{G} \\ &= \frac{\alpha^2 \Delta^2}{2} (L-1)^2 - 4\alpha^2 \Delta^2 \sum_{i=1}^{L-1} (i - L/2) \\ &\quad \times \Phi\left(\sqrt{2} \text{diag}(\mathbf{C}_z)^{-\frac{1}{2}} (i - L/2)\right) \end{aligned} \quad (47)$$

$$- \mathbf{G} \text{diag}(\mathbf{C}_z) \mathbf{G} \quad (48)$$

Here, we used (35) to obtain (47), and (41) to obtain (48).

It turns out that the diagonal approximation (48), despite its simplicity, is very accurate for DACs with medium-to-high resolution and if the OSR is relatively small (e.g., when $L \geq 4$ and $\xi \leq 4$). Unfortunately, the diagonal approximation is not sufficiently accurate for DACs with low resolution and if the OSR is high (e.g., when $L < 4$ and $\xi > 4$). Next, we derive an approximation that does not suffer from this drawback.

C. Rounding Approximation

Next, we present a second approximation of \mathbf{C}_d that is accurate if the step size Δ of the DACs is set such that the overload distortion is negligible compared to the granular distortion.

We start by noting from (23) that \mathbf{C}_x can be written as

$$\mathbf{C}_x = \alpha^2 (\mathbf{C}_z + \mathbf{C}_{ze} + \mathbf{C}_{ze}^H + \mathbf{C}_e) \quad (49)$$

where $\mathbf{C}_e = \mathbb{E}[\mathbf{e}\mathbf{e}^H] \in \mathbb{C}^{BN \times BN}$ is the covariance of \mathbf{e} and $\mathbf{C}_{ze} = \mathbb{E}[\mathbf{z}\mathbf{e}^H] \in \mathbb{C}^{BN \times BN}$; this last matrix can be expressed also as

$$\mathbf{C}_{ze} = \mathbb{E}\left[\mathbf{z}(\alpha^{-1}\mathbf{x} - \mathbf{z})^H\right] \quad (50)$$

$$= \mathbb{E}\left[\mathbf{z}(\alpha^{-1}\mathbf{G}\mathbf{z} + \alpha^{-1}\mathbf{d} - \mathbf{z})^H\right] \quad (51)$$

$$= \mathbf{C}_z(\alpha^{-1}\mathbf{G} - \mathbf{I}_{BN}). \quad (52)$$

Here, we have used that $\mathbb{E}[\mathbf{z}\mathbf{d}^H] = \mathbf{0}_{BN \times BN}$. Inserting (52) into (49), we obtain

$$\mathbf{C}_x = \alpha(\mathbf{G}\mathbf{C}_z + \mathbf{C}_z\mathbf{G}) + \alpha^2(\mathbf{C}_e - \mathbf{C}_z). \quad (53)$$

Note that the only unknown quantity in (53) is \mathbf{C}_e . Not surprisingly, evaluating \mathbf{C}_e is just as difficult as evaluating \mathbf{C}_x and no closed-form solution is available. However, if the step size Δ of the DACs is set such that the overload distortion is negligible compared to the granular distortion, the error \mathbf{e} can be accurately approximated by

$$\mathbf{e} = \alpha^{-1}\mathcal{Q}(\mathbf{z}) - \mathbf{z} \approx \mathcal{R}(\mathbf{z}) - \mathbf{z} \quad (54)$$

where the *rounding function* $\mathcal{R}(\cdot)$ is defined as follows:

$$\mathcal{R}(z) = \begin{cases} \Delta \left\lfloor \frac{z}{\Delta} + \frac{1}{2} \right\rfloor, & \text{if } L \text{ is odd} \\ \Delta \left\lfloor \frac{z}{\Delta} \right\rfloor + \frac{\Delta}{2}, & \text{if } L \text{ is even.} \end{cases} \quad (55)$$

Some comments on (54) and (55) are in order. The rounding function $\mathcal{R}(\cdot)$ describes a uniform symmetric quantizer with the same step size Δ as the uniform symmetric quantizer described by $\alpha^{-1}\mathcal{Q}(\cdot)$ but with an infinite number of quantization levels. If the input z lies within the granular region of the uniform quantizer described by $\alpha^{-1}\mathcal{Q}(\cdot)$, i.e., if $|z| \leq A_{\text{clip}}$, then $\mathcal{R}(z) = \alpha^{-1}\mathcal{Q}(z)$. If, however, the amplitude of the input z exceeds the clipping level A_{clip} , i.e., if $|z| > A_{\text{clip}}$, then $\mathcal{R}(z) \neq \alpha^{-1}\mathcal{Q}(z)$. The difference between $\alpha^{-1}\mathcal{Q}(\cdot)$ and $\mathcal{R}(\cdot)$ is illustrated in Fig. 2. Replacing $\alpha^{-1}\mathcal{Q}(\cdot)$ with $\mathcal{R}(\cdot)$ is convenient because the statistical theory of the quantizer (55) is well-investigated (see, e.g., [28], [34]–[37]) and a closed-form

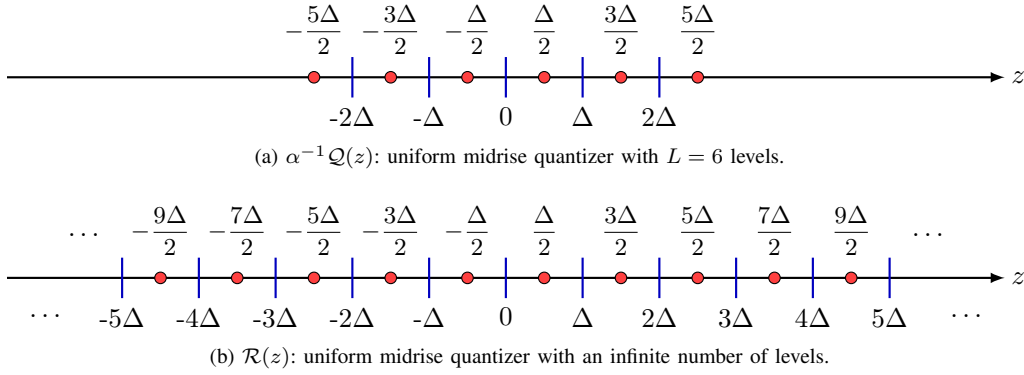


Fig. 2. Comparison between the quantization levels and thresholds associated with the rules $\alpha^{-1}\mathcal{Q}(z)$ and $\mathcal{R}(z)$; the red circles correspond to quantization labels, and the blue vertical lines correspond to quantization thresholds.

expression for the corresponding \mathbf{C}_e is known. Specifically, let e_m and e_n denote the m th and the n th entry of \mathbf{e} , respectively. Furthermore, assume that (54) holds with equality. For a midread quantizer (L odd), Sripad and Snyder showed that [34, Eq. (23)]

$$\begin{aligned} \mathbb{E}[e_m e_n^*] &= \frac{2\Delta^2}{\pi^2} \sum_{a=1}^{\infty} \sum_{b=1}^{\infty} \frac{(-1)^{a+b}}{ab} \exp\left(-\frac{\pi^2(a^2\sigma_m^2 + b^2\sigma_n^2)}{\Delta^2}\right) \\ &\quad \times \left(\sinh\left(\frac{2\pi^2 ab \sigma_{m,n}^R}{\Delta^2}\right) + j \sinh\left(\frac{2\pi^2 ab \sigma_{m,n}^I}{\Delta^2}\right) \right). \end{aligned} \quad (56)$$

For midrise quantizers (L even) it holds that (see Appendix A)

$$\begin{aligned} \mathbb{E}[e_m e_n^*] &= \frac{2\Delta^2}{\pi^2} \sum_{a=1}^{\infty} \sum_{b=1}^{\infty} \frac{1}{ab} \exp\left(-\frac{\pi^2(a^2\sigma_m^2 + b^2\sigma_n^2)}{\Delta^2}\right) \\ &\quad \times \left(\sinh\left(\frac{2\pi^2 ab \sigma_{m,n}^R}{\Delta^2}\right) + j \sinh\left(\frac{2\pi^2 ab \sigma_{m,n}^I}{\Delta^2}\right) \right). \end{aligned} \quad (57)$$

Using (56) and (57) we can write the quantization error covariance matrix for every $L \geq 2$ as

$$\begin{aligned} \mathbf{C}_e &= \frac{2\Delta^2}{\pi^2} \sum_{a=1}^{\infty} \sum_{b=1}^{\infty} \frac{\cos(\pi L)^{a+b}}{ab} \\ &\quad \times \exp\left(-\frac{\pi^2 a^2}{\Delta^2} \text{diag}(\mathbf{C}_z) \mathbf{1}_{BN \times BN}\right) \\ &\quad \times \exp\left(-\frac{\pi^2 b^2}{\Delta^2} \mathbf{1}_{BN \times BN} \text{diag}(\mathbf{C}_z)\right) \\ &\quad \times \left(\sinh\left(\frac{2\pi^2 ab}{\Delta^2} \Re\{\mathbf{C}_z\}\right) \right. \\ &\quad \left. + j \sinh\left(\frac{2\pi^2 ab}{\Delta^2} \Im\{\mathbf{C}_z\}\right) \right). \end{aligned} \quad (58)$$

We obtain the desired rounding approximation for \mathbf{C}_x by inserting (58) into (53). Then, by inserting (53) into (35) we obtain the rounding approximation for \mathbf{C}_d . Interestingly, for the case $L = 2$, it is possible to retrieve the arcsine law (45) from (58). We formalize this result in the following theorem whose proof is given in Appendix B.

Theorem 1: Assume $L = 2$, insert (58) into (53), and let

$\Delta \rightarrow \infty$. These steps yield the arcsine law (45).

As we shall see in Section V, the rounding approximation (58) turns out to be accurate independently of the resolution of the DACs, provided that Δ is chosen so that clipping occurs with low probability. Note that evaluating (58) involves computing two infinite sums. The series, however, converges rapidly because the terms decay exponentially in a and b . In what follows, we evaluate (58) by summing only the first 30 terms in both sums. As we shall demonstrate in Section V, this simplification yields accurate results.

V. NUMERICAL RESULTS

We focus on a massive MU-MIMO-OFDM system in which the number of BS antennas is $B = 128$ and the number of UEs is $U = 16$.⁵ We consider a frequency-selective Rayleigh fading channel with $L = 4$ taps and a uniform power delay profile. The OFDM numerology is inspired by a 5 MHz LTE system [38]. Specifically, the number of occupied subcarriers is $S = 300$ and the subcarrier spacing is $\Delta f = 15$ kHz. Furthermore, we assume that the occupied subcarriers are the first 150 to the left and to the right of the DC subcarrier (the DC subcarrier is not occupied). The total number of subcarriers (the size of the DFT) is $N = 1024$. Hence, the sampling rate of the DACs is $f_s = N\Delta f = 1024 \cdot 15 \cdot 10^3 = 15.36$ MHz and the OSR is $\xi = N/S = 1024/300 \approx 3.4$.⁶

Assuming that the input to the DACs at the b th antenna ($b = 1, \dots, B$) is $z_b \sim \mathcal{CN}(0, P/(\xi B))$ and that the clipping level is set according to

$$A_{\text{clip}} = \sqrt{\frac{P}{2\xi B}} \left(1 - \Phi^{-1}\left(\frac{P_{\text{clip}}}{2}\right) \right) \quad (59)$$

then the DACs will clip the signal with probability P_{clip} . In what follows, we have set the clipping level of the DACs so that $P_{\text{clip}} = 0.1\%$. This choice is suboptimal, but will enable us to accurately analyze the system using the rounding approximation (58).⁷ Furthermore, we shall see that this

⁵Our simulation framework will be made available for download from GitHub upon (possible) acceptance of the paper. The purpose is to enable interested readers to perform their own simulations with different system parameters.

⁶We shall investigate the impact of varying the OSR in Section V-D.

⁷The problem of finding optimal quantization levels and thresholds for a fixed resolution is investigated in, e.g., [39], [40].

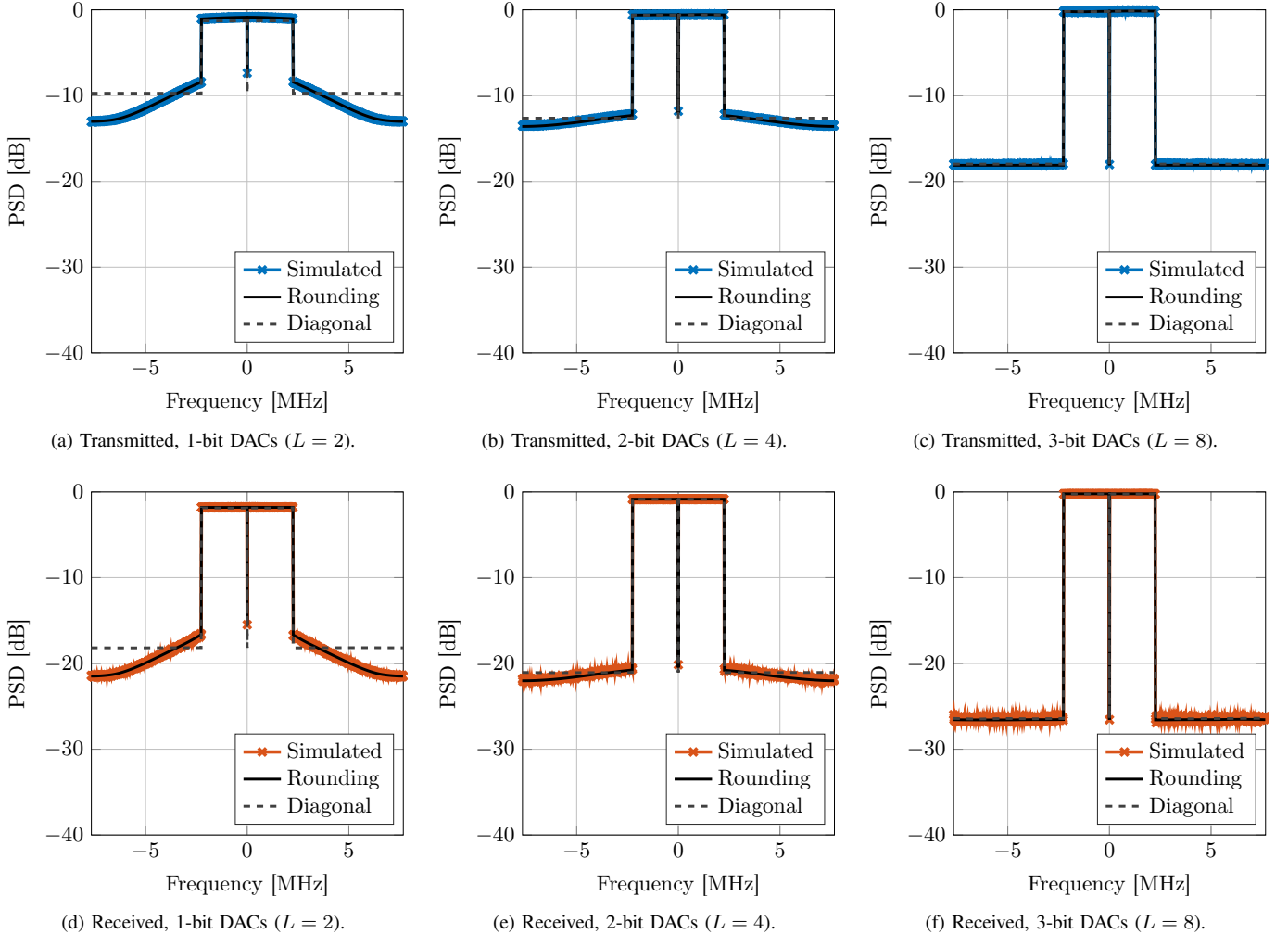


Fig. 3. PSD of the transmitted and received signal. The markers correspond to simulated values, the solid lines correspond to the rounding approximation presented in Section IV-C, and the dashed lines correspond to the diagonal approximation presented in Section IV-B.

suboptimal choice yields near-optimal (infinite resolution) performance also for DACs with low resolution.

A. Power Spectral Density

To demonstrate the accuracy of the approximations in Section IV-B and Section IV-C, we plot in Fig. 3 the PSD of the transmitted signal (averaged over the BS antennas and over 100 channel realizations) and the PSD of the received signal (averaged over the UEs and over 100 channel realizations). Here, the BS uses ZF precoding and the data vectors \mathbf{s}_k for $k \in \mathcal{S}_d$ contains QPSK symbols.⁸

Numerical simulations are compared with analytic results, which are obtained by computing the PSD of the transmitted vector \mathbf{x} and of the corresponding received vector \mathbf{y} using the diagonal approximation and the rounding approximation

⁸Recall that in Section III and Section IV, we assumed that the per-antenna DAC input was a zero-mean Gaussian random variable. This assumption holds approximately true also for the case of finite-cardinality constellations and linear precoding, because the per-antenna DAC input can be written as sum of US independent and identically distributed random variables with zero mean and finite variance. Hence, when U or S grow large, the per-antenna DAC input converges to a Gaussian random variable by the central limit theorem.

presented in Section IV-B and in Section IV-C, respectively. We note that the rounding approximation yields accurate results independently of the resolution of the DACs. We also note that the diagonal approximation results in a poor approximation of the PSD for the case $L = 2$ but yields a more accurate approximation as the number of bits increase. Indeed, if the number of bits increase, the distortion caused by the DACs becomes more spectrally white (compare Fig. 3a and Fig. 3c). We also see from the figure that the nonlinearity introduced by the low-resolution DACs causes severe OOB distortion at the BS. Interestingly, however, the relative amount of OOB distortion is smaller at the UEs than at the BS. This is because the distortion adds up incoherently at the UEs whereas the useful signal is beamformed. Nevertheless, the OOB distortion caused by the low-resolution DACs is a significant issue in practical systems as it may cause interference to UEs operating in adjacent frequency bands.

B. Error-Rate Performance

1) *Uncoded BER*: If the elements of the symbol vector \mathbf{s}_k for $k \in \mathcal{S}_d$ are drawn independently from a QPSK constellation,

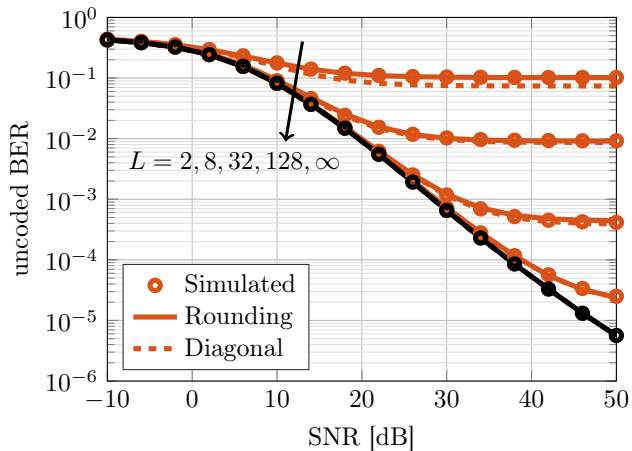
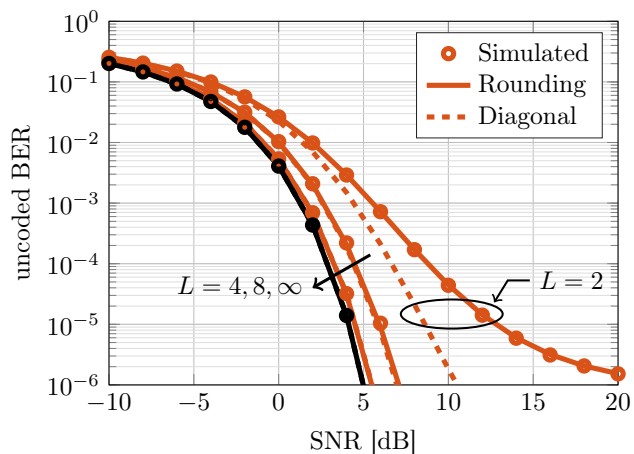
(a) Uncoded BER with QPSK; $B = 1$ and $U = 1$.(b) Uncoded BER with QPSK; $B = 128$ and $U = 16$.

Fig. 4. Uncoded BER with ZF and QPSK signaling. The markers correspond to simulated values, the solid lines correspond to the BER (60) according to the rounding approximation in Section IV-C, and the dashed lines correspond to the BER (60) according to the diagonal approximation in Section IV-B. The black lines, which overlap, correspond to the infinite-resolution case.

we can approximate the uncod BER by

$$1 - \mathbb{E} \left[\frac{1}{US} \sum_{k \in \mathcal{S}_d} \sum_{u=1}^U \Phi \left(\sqrt{\gamma_{u,k}(\hat{\mathbf{H}})} \right) \right] \quad (60)$$

where $\gamma_{u,k}(\hat{\mathbf{H}})$ is given in (31). We evaluate this quantity by using the diagonal approximation from Section IV-B and the rounding approximation from Section IV-C.

Note that for the rounding approximation or the diagonal approximation to be accurate, the number of BS antennas B does not need to be large. To illustrate this aspect, we show in Fig. 4a the uncod BER with QPSK and ZF for the single-input single-output (SISO) case (i.e., when $U = 1$ and $B = 1$) as a function of the SNR and the number of DAC bits.⁹ We compare simulated BER values with the approximation (60) and note that the rounding approximation is accurate over the entire range of SNR values. We also note that the diagonal approximation becomes more accurate as the number of DAC

⁹In the SISO-OFDM case, ZF precoding reduces to channel inversion.

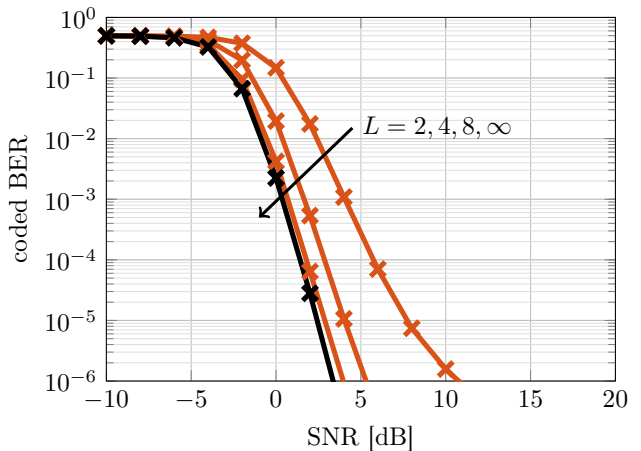
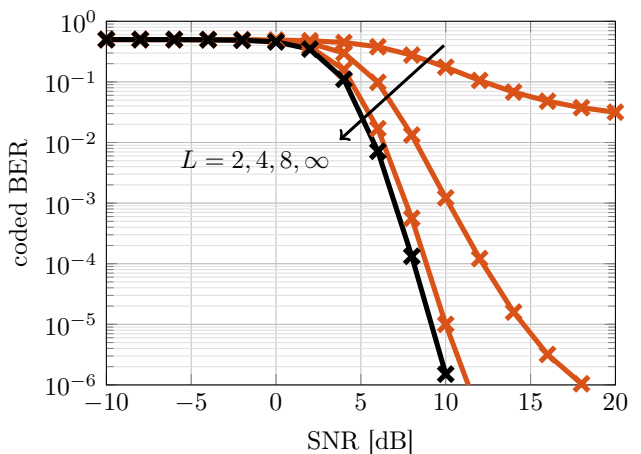
(a) Coded BER with QPSK; $B = 128$ and $U = 16$.(b) Coded BER with 16-QAM; $B = 128$ and $U = 16$.

Fig. 5. Coded BER with ZF for the case of QPSK and 16-QAM signaling. The information streams are encoded using a rate-5/6 convolutional code spanning 10 OFDM symbols. The UEs use nearest-neighbor detection and hard-input Viterbi decoding. The black lines correspond to the infinite-resolution case.

bits increase. We further note that, in the SISO-OFDM case, low uncod BERs are not supported with QPSK and low-resolution DACs. Indeed, 7–8 DAC bits are required to achieve a target BER of 10^{-4} without a significant performance degradation compared to the infinite-resolution case.

In the massive MU-MIMO-OFDM case, the large number of antennas at the BS enables a considerable reduction of the resolution of the DACs compared to the SISO-OFDM case. To illustrate this, we show in Fig. 4b the uncod BER with QPSK and ZF as a function of the SNR and the number of DAC bits for the case $B = 128$ and $U = 16$. In contrast to the SISO-OFDM case, low uncod BERs are now supported by low-resolution DACs. Indeed, an uncod BER below 10^{-4} is supported in the 1-bit-DAC case provided that the SNR exceeds 9 dB. Furthermore, only 3–4 DAC bits are necessary to close the gap to the infinite-resolution case for a target BER of 10^{-4} . This was observed for narrowband scenarios in [9].

We again note that the rounding approximation is accurate over the entire range of SNR values and independently of the number of DAC bits, and that the diagonal approximation

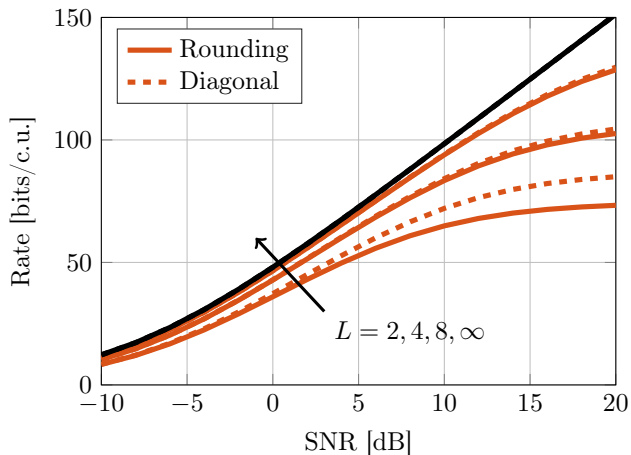


Fig. 6. Sum-rate with ZF and Gaussian signaling. The solid lines correspond to the rounding approximation in Section IV-C, the dashed lines correspond to the diagonal approximation in Section IV-B. The black lines, which overlap, correspond to the infinite-resolution case.

becomes more accurate as the number of bits increase.

2) *Coded BER*: In Fig. 5, we show the coded BER with ZF as a function of the SNR and the number of DAC bits for the case of QPSK and 16-quadrature amplitude modulation (QAM) signaling. Here, we consider the case $B = 128$ and $U = 16$, and show only simulated BER values. The BS uses a (weak) rate-5/6 convolutional code to encode the information bits (separately for each UE) over 10 OFDM symbols. Hence, a codeword spans 3000 symbols. Each UE performs symbol-wise nearest-neighbor detection and hard-input Viterbi decoding to retrieve the information streams.

We note that high-order constellations, such as 16-QAM, are supported in the massive MU-MIMO-OFDM case despite the low-resolution DACs, and that only few DAC bits are needed to close the gap to the infinite-resolution performance.

C. Achievable Rate

In Fig. 6, we show the achievable sum-rate with Gaussian signaling and ZF precoding as a function of the SNR and the number of DAC levels. The sum-rate lower bound computed using (33) is evaluated using the diagonal approximation and the rounding approximation presented in Section IV-B and Section IV-C, respectively.

We note that the diagonal approximation is accurate for the case $L \geq 4$. We further note that a high sum-rate throughput can be achieved by the massive MU-MIMO-OFDM system, despite the low-resolution of the DACs at the BS.

D. Impact of Oversampling

In Fig. 7, we investigate the impact of the OSR on the uncoded BER for the case of 1-bit DACs. Specifically, we plot the uncoded BER for the case of uncoded QPSK and ZF precoding as a function of the OSR. The SNR is set to $\rho = 10$ dB. We note that, for ZF, the uncoded BER can be considerably improved by operating the 1-bit DACs at a sampling rate higher than the symbol rate. Indeed, the

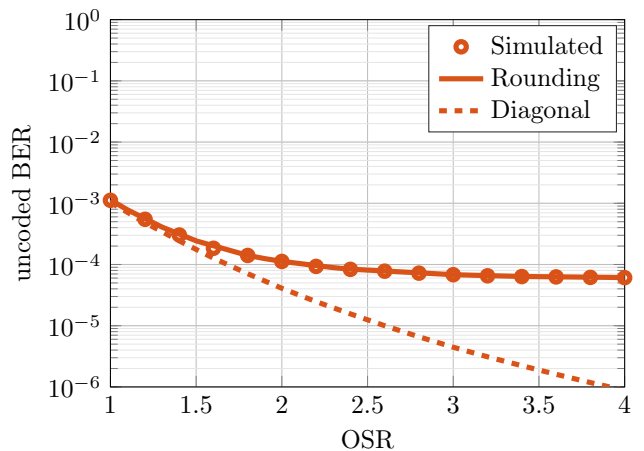


Fig. 7. Impact of the OSR on the uncoded BER for the 1-bit-DAC case; $\rho = 10$ dB, $U = 16$, $B = 128$, $S = 300$. The markers correspond to simulated values, the solid lines correspond to the BER (60) according to the rounding approximation in Section IV-C, the dashed lines correspond to the BER (60) according to the diagonal approximation in Section IV-B.

uncoded BER with ZF can be decreased by an order of magnitude compared to the symbol-rate sampling case ($\xi = 1$) by operating the 1-bit DACs at twice the symbol rate. However, further increasing the sampling rate yields only marginal performance gains.

We also note that, in the 1-bit-DAC case, the diagonal approximation is accurate for small OSRs (e.g., for $\xi < 1.4$) but underestimates significantly the BER for larger values of ξ . For higher resolution DACs, the diagonal approximation is accurate also for high OSRs (see, e.g., Fig. 4b).

VI. CONCLUSIONS

We have characterized the performance in terms of uncoded/coded BER and achievable sum-rate throughput of a massive MU-MIMO-OFDM downlink system, in which the BS is equipped with low-resolution DACs and uses linear precoding. Using Bussgang's theorem, we have derived lower bound on the achievable sum-rate and accurate approximations for the uncoded BER with QPSK.

We have developed two different approximations for the distortion caused by the low-resolution DACs. The first *diagonal approximation* is an easy-to-evaluate approximation that assumes that the DAC distortion is spatially and spectrally white. This approximation turns out to be accurate for moderate-to-high DAC resolutions and when the OSR is not too high. The second *rounding approximation*, which ignores the overload distortion caused by the DACs, is a more involved approximation that is accurate for DACs of arbitrary resolution and for any OSR. We also prove that the rounding approximation can be made exact in the 1-bit-DAC case by taking Δ in (58) to infinity.

By means of numerical simulations, we have illustrated that low uncoded and coded BERs and high sum-rate throughputs are achievable by massive MU-MIMO-OFDM systems, despite the severe nonlinearity introduced by low-resolution DACs. Our results suggest that for the SISO case, approximately 7–8 DAC bits are required to achieve an uncoded BER of 10^{-4}

with negligible performance penalty compared to the case of ideal DACs. In contrast, for a massive MU-MIMO-OFDM system with a 128-antenna BS serving simultaneously 16 UEs, only 3–4 DAC bits are required to achieve an uncoded BER of 10^{-4} with a negligible performance penalty compared to the infinite-resolution case.

In practice, OOB emissions caused by the low-resolution DACs could prevent their use in practical systems. Developing methods for reducing OOB emissions is part of ongoing work.

APPENDIX A DERIVATION OF (57)

It can be shown (see, e.g., [37, Eq. (9.7)]) that for midtread rounding quantizers it holds that

$$\begin{aligned} \mathbb{E}[e_m^C e_n^R] &= \frac{\Delta^2}{2\pi^2} \sum_{a=1}^{\infty} \sum_{b=1}^{\infty} \frac{(-1)^{a+b}}{ab} \\ &\times \left(\Re \left\{ \varphi_{z_m^C, z_n^R} \left(\frac{2\pi a}{\Delta}, -\frac{2\pi b}{\Delta} \right) \right\} \right. \\ &\left. - \Re \left\{ \varphi_{z_m^C, z_n^R} \left(\frac{2\pi a}{\Delta}, \frac{2\pi b}{\Delta} \right) \right\} \right) \end{aligned} \quad (61)$$

where $\varphi_{z_m^C, z_n^R}(u, v) = \mathbb{E}[e^{j(uz_m^C + vz_n^R)}]$ is the characteristic function of $[z_m^C, z_n^R]^T$, where $C \in \{R, I\}$.

Note that by adding a constant $\Delta/2$ to the input of a midtread rounding quantizer, the output of said midtread rounding quantizer equals exactly the output of a midrise rounding quantizer for the case when no constant has been added. Further note that $\varphi_{z_m^C + \Delta/2, z_n^R + \Delta/2}(u, v) = e^{j\Delta(u+v)/2} \varphi_{z_m^C, z_n^R}(u, v)$. Hence, for midrise rounding quantizers, it holds that

$$\begin{aligned} \mathbb{E}[e_m^C e_n^R] &= \frac{\Delta^2}{2\pi^2} \sum_{a=1}^{\infty} \sum_{b=1}^{\infty} \frac{(-1)^{a+b}}{ab} \\ &\times \left(\Re \left\{ e^{j\pi(a-b)} \varphi_{z_m^C, z_n^R} \left(\frac{2\pi a}{\Delta}, -\frac{2\pi b}{\Delta} \right) \right\} \right. \\ &\left. - \Re \left\{ e^{j\pi(a+b)} \varphi_{z_m^C, z_n^R} \left(\frac{2\pi a}{\Delta}, \frac{2\pi b}{\Delta} \right) \right\} \right). \end{aligned} \quad (62)$$

In our case, $[z_m^C, z_n^R]^T$ is a zero-mean Gaussian random vector for which it holds that

$$\varphi_{z_m^C, z_n^R}(u, v) = \exp\left(-\frac{1}{4}(u\sigma_m^2 + 4uv\sigma_{m,n}^C + v\sigma_n^2)\right). \quad (63)$$

Using (63), we simplify (62) as follows:

$$\begin{aligned} \mathbb{E}[e_m^C e_n^R] &= \frac{\Delta^2}{2\pi^2} \sum_{a=1}^{\infty} \sum_{b=1}^{\infty} \frac{1}{ab} \exp\left(-\frac{\pi^2(a^2\sigma_m^2 + b^2\sigma_n^2)}{\Delta^2}\right) \\ &\times \left(\exp\left(\frac{2\pi^2 ab \sigma_{m,n}^C}{\Delta^2}\right) - \exp\left(-\frac{2\pi^2 ab \sigma_{m,n}^C}{\Delta^2}\right) \right) \\ &= \frac{\Delta^2}{\pi^2} \sum_{a=1}^{\infty} \sum_{b=1}^{\infty} \frac{1}{ab} \exp\left(-\frac{\pi^2(a^2\sigma_m^2 + b^2\sigma_n^2)}{\Delta^2}\right) \\ &\times \sinh\left(\frac{2\pi^2 ab \sigma_{m,n}^C}{\Delta^2}\right). \end{aligned} \quad (65)$$

Here, (64) holds because $\Re\{e^{j\pi(a-b)}\} = \cos(\pi(a-b)) = (-1)^{a+b}$ and $\Re\{e^{j\pi(a+b)}\} = \cos(\pi(a+b)) = (-1)^{a+b}$ for $a \in \mathbb{Z}$ and $b \in \mathbb{Z}$. We obtain (65) by noting that $2\sinh(x) = e^x - e^{-x}$. From (65) we finally obtain the desired result (57) by noting that $\mathbb{E}[e_m^R e_n^*] = 2(\mathbb{E}[e_m^R e_n^R] + j\mathbb{E}[e_m^I e_n^R])$, which holds as the input to the DACs is a circularly-symmetric Gaussian random variable.

APPENDIX B PROOF OF THEOREM 1

Recall that, for the case $L = 2$, α is given by (9) and $\text{diag}(\mathbf{g})$ is given by (27). Hence, since $P < \infty$, it follows from (53) that

$$\lim_{\Delta \rightarrow \infty} \mathbf{C}_x = \lim_{\Delta \rightarrow \infty} \frac{2P}{\Delta^2 \xi B} \mathbf{C}_e. \quad (66)$$

Hence, to prove Theorem 1, we need to show that the entry on the m th row and on the n th column of the RHS of (66) equals the RHS of (44), if we use (58) to evaluate \mathbf{C}_e . Let $u_a = a/\Delta$ and $v_b = b/\Delta$. Then, we can write the entry on the m th row and n th column of the RHS of (66) as

$$\begin{aligned} \lim_{\Delta \rightarrow \infty} [\mathbf{C}_x]_{m,n} &= \lim_{\Delta \rightarrow \infty} \frac{4P}{\pi^2 \Delta^2 \xi B} \\ &\times \sum_{a=1}^{\infty} \sum_{b=1}^{\infty} \frac{1}{u_a v_b} \exp(-\pi^2(u_a^2 \sigma_m^2 + v_b^2 \sigma_n^2)) \\ &\times (\sinh(2\pi^2 u_a v_b \sigma_{m,n}^R) + j \sinh(2\pi^2 u_a v_b \sigma_{m,n}^I)) \quad (67) \\ &= \frac{4P}{\pi^2 \xi B} \int_0^{\infty} \int_0^{\infty} \frac{1}{uv} \exp(-\pi^2(u^2 \sigma_m^2 + v^2 \sigma_n^2)) \\ &\times (\sinh(2\pi^2 uv \sigma_{m,n}^R) + j \sinh(2\pi^2 uv \sigma_{m,n}^I)) du dv \quad (68) \\ &= \frac{2P}{\pi \xi B} \left(\arcsin\left(\frac{\sigma_{m,n}^R}{\sigma_m \sigma_n}\right) + j \arcsin\left(\frac{\sigma_{m,n}^I}{\sigma_m \sigma_n}\right) \right). \end{aligned} \quad (69)$$

Here, to obtain (67), we replaced $[\mathbf{C}_e]_{m,n}$ with (57). To obtain (68), we noted that (67) is a two-dimensional Riemann sum, which, by definition, can be written as the two-dimensional integral in (68). Finally, to obtain (69), we used that

$$\begin{aligned} \frac{2}{\pi} \int_0^{\infty} \int_0^{\infty} \frac{1}{uv} \exp(-\pi^2(u^2 \sigma_m^2 + v^2 \sigma_n^2)) \\ \times \sinh(2\pi^2 uv \sigma_{m,n}^C) du dv = \arcsin\left(\frac{\sigma_{m,n}^C}{\sigma_m \sigma_n}\right). \end{aligned} \quad (70)$$

We note that (69) is equal to the RHS of (44). This concludes the proof.

ACKNOWLEDGEMENTS

The authors would like to thank Dr. D. Astely and Dr. U. Gustavsson at Ericsson Research for fruitful discussions. The work of S. Jacobsson and G. Durisi was supported by the Swedish Foundation for Strategic Research under grant ID14-0022, and by the Swedish Governmental Agency for Innovation Systems (VINNOVA) within the competence center ChaseOn. The work of C. Studer was supported by Xilinx, Inc. and by the US National Science Foundation (NSF) under grants ECCS-1408006, CCF-1535897, CAREER CCF-1652065, and CNS-1717559.

REFERENCES

- [1] S. Jacobsson, G. Durisi, M. Coldrey, and C. Studer, "Massive MU-MIMO-OFDM downlink with one-bit DACs and linear precoding," in *Proc. IEEE Global Telecommun. Conf. (GLOBECOM)*, 2017, to appear.
- [2] F. Boccardi, R. W. Heath Jr., A. Lozano, T. L. Marzetta, and P. Popovski, "Five disruptive technology directions for 5G," *IEEE Commun. Mag.*, vol. 52, no. 2, pp. 74–80, Feb. 2014.
- [3] T. L. Marzetta, "Noncooperative cellular wireless with unlimited numbers of base station antennas," *IEEE Trans. Wireless Commun.*, vol. 9, no. 11, pp. 3590–3600, Nov. 2010.
- [4] F. Rusek, D. Persson, B. Kiong, E. G. Larsson, T. L. Marzetta, O. Edfors, and F. Tufvesson, "Scaling up MIMO: Opportunities and challenges with very large large arrays," *IEEE Signal Process. Mag.*, vol. 30, no. 1, pp. 40–60, Jan. 2013.
- [5] E. G. Larsson, F. Tufvesson, O. Edfors, and T. L. Marzetta, "Massive MIMO for next generation wireless systems," *IEEE Commun. Mag.*, vol. 52, no. 2, pp. 186–195, Feb. 2014.
- [6] L. Lu, G. Ye Li, A. L. Swindlehurst, A. Ashikhmin, and R. Zhang, "An overview of massive MIMO: Benefits and challenges," *IEEE J. Sel. Topics Signal Process.*, vol. 8, no. 5, pp. 742–758, Oct. 2014.
- [7] A. K. Saxena, I. Fijalkow, and A. L. Swindlehurst, "Analysis of one-bit quantized precoding for the multiuser massive MIMO downlink," *IEEE Trans. Signal Process.*, vol. 65, no. 17, pp. 4624–4634, Sep. 2017.
- [8] Y. Li, C. Tao, A. L. Swindlehurst, A. Mezghani, and L. Liu, "Downlink achievable rate analysis in massive MIMO systems with one-bit DACs," *IEEE Commun. Lett.*, vol. 21, no. 7, pp. 1669–1672, Jul. 2017.
- [9] S. Jacobsson, G. Durisi, M. Coldrey, T. Goldstein, and C. Studer, "Quantized precoding for massive MU-MIMO," *IEEE Trans. Commun.*, 2017, to appear.
- [10] —, "Nonlinear 1-bit precoding for massive MU-MIMO with higher-order modulation," in *Proc. Asilomar Conf. Signals, Syst., Comput.*, Pacific Grove, CA, USA, Nov. 2016, pp. 763–767.
- [11] H. Jedda, J. A. Nossek, and A. Mezghani, "Minimum BER precoding in 1-bit massive MIMO systems," in *IEEE Sensor Array and Multichannel Signal Process. Workshop (SAM)*, Rio de Janeiro, Brazil, Jul. 2016.
- [12] O. Castañeda, S. Jacobsson, G. Durisi, M. Coldrey, T. Goldstein, and C. Studer, "1-bit massive MU-MIMO precoding in VLSI," *IEEE J. Emerging Sel. Topics Circuits Syst.*, 2017, to appear.
- [13] A. L. Swindlehurst, A. K. Saxena, A. Mezghani, and I. Fijalkow, "Minimum probability-of-error perturbation precoding for the one-bit massive MIMO downlink," in *Proc. IEEE Int. Conf. Acoust., Speech, Signal Process. (ICASSP)*, New Orleans, LA, USA, Mar. 2017, pp. 6483–6487.
- [14] J. J. Bussgang, "Crosscorrelation functions of amplitude-distorted Gaussian signals," Res. Lab. Elec., Cambridge, MA, Tech. Rep. 216, Mar. 1952.
- [15] H. E. Rowe, "Memoryless nonlinearities with Gaussian inputs: Elementary results," *Bell Labs Tech. J.*, vol. 61, no. 7, pp. 1519–1525, Sep. 1982.
- [16] J. H. Van Vleck and D. Middleton, "The spectrum of clipped noise," *Proc. IEEE*, vol. 54, no. 1, pp. 2–19, Jan. 1966.
- [17] C. Studer, M. Wenk, and A. Burg, "MIMO transmission with residual transmit-RF impairments," in *Proc. Int. ITG Workshop on Smart Antennas (WSA)*, Bremen, Germany, Feb. 2010, pp. 189–196.
- [18] U. Gustavsson, C. Sánchez-Perez, T. Eriksson, F. Athley, G. Durisi, P. Landin, K. Hausmair, C. Fager, and L. Svensson, "On the impact of hardware impairments on massive MIMO," in *Proc. IEEE Global Telecommun. Conf. (GLOBECOM)*, Austin, TX, USA, Dec. 2014, pp. 294–300.
- [19] E. Björnson, M. Matthaiou, and M. Debbah, "Massive MIMO with non-ideal arbitrary arrays: Hardware scaling laws and circuit-aware design," *IEEE Trans. Wireless Commun.*, vol. 14, no. 8, pp. 4353–4368, Apr. 2015.
- [20] X. Zhang, M. Matthaiou, M. Coldrey, and E. Björnson, "Impact of residual transmit RF impairments on training-based MIMO systems," *IEEE Trans. Commun.*, vol. 63, no. 8, pp. 2899–2911, Aug. 2015.
- [21] C.-K. Wen, C.-J. Wang, S. Jin, K.-K. Wong, and P. Ting, "Bayes-optimal joint channel-and-data estimation for massive MIMO with low-precision ADCs," *IEEE Trans. Signal Process.*, vol. 64, no. 10, pp. 2541–2556, Jul. 2015.
- [22] S. Jacobsson, G. Durisi, M. Coldrey, U. Gustavsson, and C. Studer, "Throughput analysis of massive MIMO uplink with low-resolution ADCs," *IEEE Trans. Wireless Commun.*, vol. 16, no. 6, pp. 4038–4051, Jun. 2017.
- [23] C. Studer and G. Durisi, "Quantized massive MU-MIMO-OFDM uplink," *IEEE Trans. Commun.*, vol. 64, no. 6, pp. 2387–2399, Jun. 2016.
- [24] C. Mollén, J. Choi, E. G. Larsson, and R. W. Heath Jr., "Uplink performance of wideband massive MIMO with one-bit ADCs," *IEEE Trans. Wireless Commun.*, vol. 16, no. 1, pp. 87–100, Oct. 2016.
- [25] A. Mezghani, R. Ghiat, and J. A. Nossek, "Transmit processing with low resolution D/A-converters," in *Proc. IEEE Int. Conf. Electron., Circuits, Syst. (ICECS)*, Yasmine Hammamet, Tunisia, Dec. 2009, pp. 683–686.
- [26] R. D. J. Guerreiro and P. Montezuma, "Use of 1-bit digital-to-analogue converters in massive MIMO systems," *IEEE Electron. Lett.*, vol. 52, no. 9, pp. 778–779, Apr. 2016.
- [27] F. Maloberti, *Data converters*. Springer, Mar. 2007.
- [28] R. M. Gray and D. L. Neuhoff, "Quantization," *IEEE Trans. Inf. Theory*, vol. 44, no. 6, pp. 2325–2383, Oct. 1998.
- [29] S. Gunnarsson, M. Bortas, Y. Huang, C.-M. Chen, L. Van der Pierre, and O. Edfors, "Lousy processing increases energy efficiency in massive MIMO systems," in *Proc. Eur. Conf. Netw. Commun. (EuCNC)*, Oulu, Finland, Jun. 2017.
- [30] M. Joham, W. Utschick, and J. A. Nossek, "Linear transmit processing in MIMO communications systems," *IEEE Trans. Signal Process.*, vol. 53, no. 8, pp. 2700–2712, Aug. 2005.
- [31] A. Lapidoto, "Nearest neighbor decoding for additive non-Gaussian noise channels," *IEEE Trans. Inf. Theory*, vol. 42, no. 5, pp. 1520–1529, Sep. 1996.
- [32] W. Zhang, "A general framework for transmission with transceiver distortion and some applications," *IEEE Trans. Commun.*, vol. 60, no. 2, pp. 384–399, Feb. 2012.
- [33] H. A. Fayed and A. F. Atiya, "An evaluation of the integral of the product of the error function and the normal probability density with application to the bivariate normal integral," *Math. Comput.*, vol. 83, no. 285, pp. 235–250, Jan. 2014.
- [34] A. B. Sripad and D. L. Snyder, "A necessary and sufficient condition for quantization errors to be uniform and white," *IEEE Trans. Acoust., Speech, Signal Process.*, vol. 25, no. 5, pp. 442–448, Oct. 1977.
- [35] B. Widrow, "Statistical analysis of amplitude quantized sampled data systems," *Trans. Am. Inst. Electr. Eng. Pt. II: Appl. Ind.*, vol. 79, no. 6, pp. 555–568, Jan. 1961.
- [36] S. P. Lipshitz, R. A. Wannamaker, and J. Vanderkooy, "Quantization and dither: A theoretical survey," *J. Audio Eng. Soc.*, vol. 40, no. 5, pp. 355–375, May 1992.
- [37] B. Widrow and I. Kollár, *Quantization Noise: Roundoff Error in Digital Computation, Signal Processing, Control, and Communications*. Cambridge, UK: Cambridge Univ. Press, 2008.
- [38] 3GPP, "LTE; evolved universal terrestrial radio access (E-UTRA); user equipment (UE) radio transmission and reception," Apr. 2017, TS 36.101 version 14.3.0 Rel. 14.
- [39] J. Max, "Quantizing for minimum distortion," *IRE Trans. Inf. Theory*, vol. 6, no. 1, pp. 7–12, Mar. 1960.
- [40] N. Al-Dhahir and J. M. Cioffi, "On the uniform ADC bit precision and clip level computation for a Gaussian signal," *IEEE Trans. Signal Process.*, vol. 44, no. 2, pp. 434–438, Feb. 1996.